Catalysis Science & Technology

PAPER

View Article Online
View Journal | View Issue

Cite this: *Catal. Sci. Technol.*, 2016, 6, 7203

Interaction of alkali acetates with silica supported PdAu†‡§

Elisabeth K. Hanrieder, Andreas Jentys* and Johannes A. Lercher*

Received 6th June 2016,
Accepted 14th July 2016

DOI: 10.1039/c6cy01228k

www.rsc.org/catalysis

The temperature dependence of the interaction of PdAu alloy particles with alkali acetate promoters (MOAc; M^+ = Li^+, Na^+, K^+, Cs^+) was studied by X-ray absorption and infrared spectroscopy as well as *in situ* X-ray diffraction. Alkali acetate promotion on PdAu particles results in irreversible enlargements of the Pd–Pd distances upon heating compared to promoter free PdAu/SiO_2. The promoter induces the migration of Pd to the metal particle surface and the formation of a mixed Pd/M^+–O layer on the surface of the bimetallic PdAu particles. This structure enhances catalytic reactions by electronically and geometrically modifying the PdAu surface.

1. Introduction

Bimetallic alloy catalysts have attracted significant attention as the presence of a second metal allows to subtly modify activity and selectivity.[1–3] Metal combinations exhibiting a continuous range of solubility such as Pd and Au,[4] where both elements have similar electronegativity, metal radii and number of valence electrons have been found to be particularly rewarding.[5] Formation heats of PdAu alloys are exothermic over the entire composition range, pointing to attractive interactions between the alloy constituents and to a tendency to form long range ordered phases[6] such as Au_3Pd (stable up to ~850 °C), Au_1Pd_1 (stable up to ~100 °C) and $AuPd_3$ (stable up to ~870 °C).[7,8] Lattice parameters of these bimetallic phases follow Vegard's law and vary from 0.389 nm to 0.406 nm as a function of the composition for PdAu particles with a small negative deviation of 0.0004 nm at about 30 at% Pd.[9]

However, the Pd/Au composition of the bulk and the catalytically active surface can differ markedly[4,10] due to differences in surface free energies of Pd (2.043 J m^{-2})[11] and Au (1.626 J m^{-2}).[12] Au preferentially decorates the surface in PdAu particles upon heating in vacuum,[13] however, we have recently shown that the presence of potassium acetate (KOAc) on PdAu, the trend reverses to surface segregation of Pd under reaction conditions of vinyl acetate (VA) synthesis.[14,15] This change is induced by the strong interaction of KOAc with Pd.[14,16,17]

The activity and selectivity of the structure sensitive VA synthesis reaction are determined by the relative arrangement of active Pd monomers suitably spaced by inert Au atoms on the solid surface.[18] Thus, the rate-enhancing effect of KOAc in VA synthesis is attributed to a geometric reordering in PdAu particles. It is unclear, however, whether such local reordering induced by KOAc exists also under "non-reactive" conditions and which impact the nature of the alkali metal has on this process. To address these questions, we systematically studied the impact of the promoter metal nature on the local environment of Pd and Au using a combination of bulk and surface sensitive techniques and to explore the impact on activity and selectivity for the structure sensitive VA synthesis.

2. Experimental

2.1. Synthesis

PdAu/SiO_2 with an atomic Pd/Au ratio of 2.0 was prepared *via* incipient wetness impregnation.[19] $HAuCl_4$ and $PdCl_2$ were dissolved in bidistilled water (1 mL g^{-1} support) and impregnated on SiO_2 (HDK®). Subsequent precipitation with sodium carbonate and washing with ammonia solution (pH 8) was carried out to remove chloride ions from the precipitated metal salts. The PdAu/SiO_2 precursors were reduced in flowing H_2 (100 mL min^{-1}) at 300 °C for 1 h (5 °C min^{-1}). The Pd and Au metal loading was 1.5 wt% each for all catalysts. The monometallic references Pd/SiO_2 and Au/SiO_2 were synthesized with a metal loading of 3 wt% in the same way. Li^+, Na^+, K^+ and Cs^+ were added as acetates to PdAu/SiO_2, Pd/SiO_2 and Au/SiO_2. For the K^+ containing catalysts, different counter ions were used including acetate (KOAc), hydroxide (KOH), carbonate (K_2CO_3) and oxalate ($K_2C_2O_4$), while

Department of Chemistry and Catalysis Research Center, Technische Universität München, Lichtenbergstr. 4, 85747 Garching, Germany. E-mail: jentys@tum.de, johannes.lercher@ch.tum.de; Fax: +49 89 289 13544; Tel: +49 89 289 13538, +49 89 289 13540

† The authors declare no competing financial interest.

‡ All authors have given approval to the final version of the manuscript.

§ Electronic supplementary information (ESI) available: Additional information about EXAFS fit results, IR of adsorbed CO, XRD and *in situ* IR spectra are listed. See DOI: 10.1039/c6cy01228k

maintaining a constant potassium concentration of 1.28 mmol g^{-1} catalyst. Representative TEM pictures including particle size distributions of $PdAu/SiO_2$ and on $PdAu/KOAc/SiO_2$ are shown in Fig. S1, ESI.§

2.2. Elemental analysis

Potassium, palladium and gold contents were determined by atomic absorption spectroscopy (AAS). For this, 50 mg of catalyst was dissolved in a mixture containing 48% hydrofluoric acid and nitro-hydrochloric acid. The spectrometer used was a Solaar M5 Dual Flame graphite furnace AAS (ThermoFisher).

2.3. X-ray powder diffraction

X-Ray powder diffraction measurements were conducted on a Philips X'Pert Pro PW 3040/60 system in Bragg–Brentano geometry (θ–2θ-goniometer) using Cu K_α radiation (0.154056 nm) generated at 45 kV and 40 mA and a solid state detector (X'Celerator). *In situ* experiments were carried out in an Anton Paar HTK 1200 cell under flowing gas atmosphere (N_2, H_2, synthetic air). The XRD patterns were measured in a 2θ range of 5–70° with a step size of 0.019° s^{-1}. Samples were annealed at 140 °C or 300 °C and cooled to ambient temperature with a heating and cooling rate of 3 °C min^{-1}. The two temperature programs are shown in Fig. S2, ESI.§ The XRD patterns obtained were analyzed with High Score Plus (PANalytical) and compared to Au and Pd references from the Crystallographic Open Database (COD). Alloy compositions were calculated by applying fitted peak positions to Vegard's law.[20]

2.4. IR spectroscopy of adsorbed CO

The IR spectra were recorded on a Vertex 70 spectrometer from Bruker Optics at a resolution of 4 cm^{-1} collecting 100 scans. Samples were pressed into self-supporting wafers (~10 mg cm^{-2}), activated in vacuum (~1.0×10^{-7} mbar) and reduced in static H_2 (1000 mbar) at 300 °C for 1 h with a heating rate of 5 °C min^{-1}. The samples were outgassed at 300 °C in vacuum for 30 min to remove Pd hydrides before the temperature was decreased either to 100 °C or to −150 °C in 5 mbar He (added to improve the thermal conductivity) to record a spectrum of the activated sample. 1.0 mbar CO was introduced and spectra were recorded until the CO adsorption–desorption equilibrium was established.

Analysis of the spectra was carried out using the software Grams AI. The spectra were background corrected and subtracted from the background corrected spectrum of the activated sample to isolate the infrared bands of adsorbed CO. These subtracted spectra were normalized to the integrated area of Si–O overtones between 2107 and 1741 cm^{-1} of the activated sample. The intensities of the CO absorption bands were evaluated by fitting with a mixed 50/50 Gaussian–Lorentzian function.

2.5. X-ray absorption spectroscopy at the Pd-K and Au-L_3-edge

X-Ray absorption spectra were measured at HASYLAB (DESY, Hamburg/Germany) on the beamlines X1 and C (electron energy of 4.5 GeV, average current of 100 mA). Spectra were recorded in transmission mode at the Pd-K edge (E_0 = 24 350 eV) using Si(311) crystals and Au-L_3 edge (E_0 = 11 919 eV) using Si(111) crystals. The samples were pressed into self-supporting wafers with weights to obtain a total absorbance of 2.0 to optimize the signal to noise ratio. The samples were activated at 300 °C with 5 °C min^{-1} in He (100 mL min^{-1}), reduced at 300 °C for 1 h in H_2 and flushed with 150 mL min^{-1} He before cooling to liquid nitrogen temperature to record 2–3 spectra per sample.

EXAFS data were processed with IFEFFIT, Athena and Artemis.[21] The scattering contributions of the pre and post-edge were removed by a third-order polynomial function. The oscillations were weighted by k^2 and Fourier transformed within the limits k = 2.1–12 $Å^{-1}$ for the Pd-K edge and k = 2.8–12 $Å^{-1}$ for the Au-L_3 edge. The EXAFS functions from $PdAu/LiOAc/SiO_2$ are compared to $PdAu/SiO_2$ in Fig. S3, ESI.§

The amplitude reduction factor S_o^2 was determined for bulk references and set to 0.9 for Au and 1.0 for Pd during analysis. Multiple-edge fitting was carried out with following constraints.

$$N_{AuPd} = N_{PdAu} x_{Pd}/x_{Au} \quad (1)$$

$$r_{AuPd} = r_{PdAu} \quad (2)$$

$$\sigma_{AuPd} = \sigma_{PdAu} \quad (3)$$

x being the molar fraction of the element in the bimetallic sample. The contribution of incorporated alkali metal ions in PdAu particles was evaluated applying first shell analysis.

3. Results and discussion

3.1. Pd surface enrichment on PdAu particles induced by MOAc (M^+ = Li^+, Na^+, K^+, Cs^+)

Electronic and geometric effects of MOAc promotor (M^+ = Li^+, Na^+, K^+ and Cs^+) on surface properties of the PdAu particles were studied by IR spectra of CO adsorbed at −150 °C on $PdAu/MOAc/SiO_2$. Bands for CO adsorbed on OH groups of SiO_2 at 2157 cm^{-1} [22,23] and with trace concentrations of cations at 2184 cm^{-1} [24,25] were observed. The stretching frequency ν(C═O) of physisorbed CO appeared at 2135 cm^{-1}.[26,27] CO adsorbed on Au atoms in a linear mode at 2104 cm^{-1},[2,28–30] while on Pd atoms, both linear and bridged adsorption modes were observed at 2109 cm^{-1} and 1991 cm^{-1}, respectively.[29,31–33]

On bimetallic PdAu surfaces the broad band between 2135–2000 cm^{-1} consists of two contributions for CO linearly bound to Au (2128/2106 cm^{-1}) and of two bands for CO linearly bound to Pd (2084/2063 cm^{-1}). The band at 2128 cm^{-1} is attributed to CO on Au atoms surrounded by Pd (linear CO

on "Au next to Pd") and the band at 2106 cm^{-1} is assigned to CO linearly bound on Au atoms in proximity to other Au atoms (linear CO on "Au next to Au"). The band at 2084 cm^{-1} is attributed to CO chemisorbed on larger Pd islands (linear CO on "Pd next to Pd") and the band at 2063 cm^{-1} to linearly adsorbed CO on Pd atoms surrounded by Au (linear CO on "Pd next to Au").[34]

Alloying of Pd with Au shifts electron density towards the element with the larger fraction of empty valence states.[35] Lee *et al.* suggested that Au gains sp-type electrons and loses d-electrons, whereas Pd loses sp-electrons and gains d-electrons.[36] The increase in the electron density in the d-states of Pd leads to a stronger electron (back-)donation into the antibonding π* orbitals of CO, which shifts the CO stretching vibration to lower wavenumbers.[29] In contrast, the band of linearly adsorbed CO on Au in proximity to Pd appeared at higher wavenumbers, as the electron density in the d-bands of Au decreases by the interaction with Pd.[14]

Fig. 1 presents the IR spectra of CO adsorbed on PdAu/MOAc/SiO_2 (M^+ = Li^+, Na^+, K^+, Cs^+) at −150 °C.

The presence of MOAc on PdAu led (i) to a shift of the stretching frequencies assigned to linear and bridged CO to lower wavenumbers, (ii) to a broadening of linear and bridged bands of adsorbed CO, (iii) to a preferential adsorption of CO on bridged rather than on linear sites and (iv) to a change in the relative band areas of linearly adsorbed CO on Au and Pd. These changes increased with increasing alkali metal radius from Li^+, Na^+, K^+ to Cs^+.

The gradual red-shift (Fig. 2) of the linear and bridged CO bands from Li^+ to Cs^+ promoted PdAu is attributed to the electron donating effect of the promoter towards the metal d-orbitals. This leads to an enhanced back donation from Pd and Au into the 2π* antibonding orbitals of CO, which strengthens the metal–carbon bond, but weakens the carbon–oxygen bond.[37–42]

The impact of the metal cation increased from Li^+ (hard Lewis acid site) to Cs^+ (soft Lewis acid site). The cations are

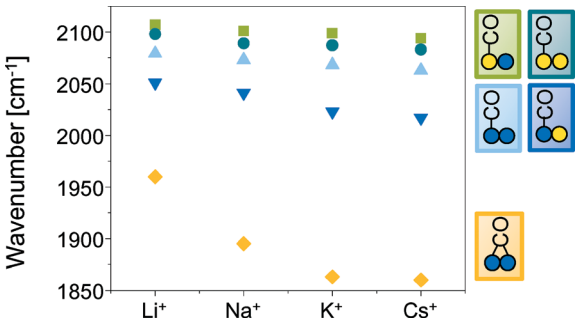

Fig. 2 IR band positions [cm^{-1}] of linearly and bridged adsorbed CO in dependence of the promoter M^+ in PdAu/MOAc/SiO_2 (M^+ = Li^+, Na^+, K^+, Cs^+).

considered to produce a long-range electronic effect mediated by the substrate, which is effective over several interatomic distances.[40] These electronic effects of MOAc on PdAu as well as the physical presence of cation are able to reduce the intermolecular dipole–dipole coupling of CO, which is manifested by an increase in the wavenumber of the ν(C═O) vibration with increasing surface coverage.[43]

Finally the decrease in the frequency of the CO stretching vibration could be related to the reduction of the concentration of continuous Pd adsorption sites for CO by the presence of K^+ and thus the extent of dipole–dipole coupling.[44] The electron-donating alkali metals M^+ increase the binding energy of reactive molecules to the metal by enhancing back donation, leading, *e.g.*, to a higher heat of adsorption of CO.[37,38,41] Therefore, we attribute the shift of the CO stretching vibration to electronic effects resulting from the interaction with MOAc.

The increased widths at half height of the CO band hints to an enhanced surface heterogeneity induced by the presence of MOAc, which resulted in an enhanced disorder in the adsorbed CO overlayer. The continuous shift of CO bands results from the varying distances between CO to M^+. The shorter the distance between CO and M^+, the larger the CO band shift.[39]

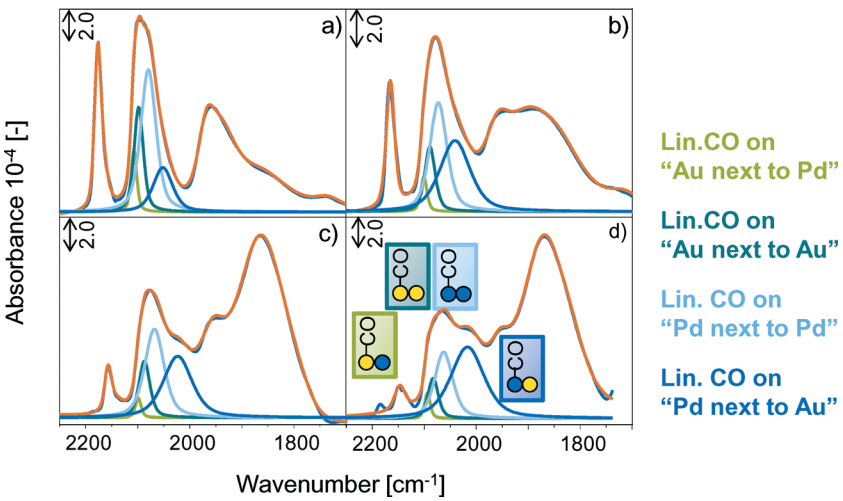

Fig. 1 IR spectra of 1.0 mbar CO adsorbed on PdAu/SiO_2 promoted with (a) LiOAc, (b) NaOAc, (c) KOAc and (d) CsOAc at −150 °C. Green lines represent linearly adsorbed CO on Au, blue lines CO on Pd.

The preferential adsorption of CO in bridged rather than linear form and the change in integral intensity of linearly adsorbed CO on Au and Pd indicates a MOAc induced enrichment of Pd on the bimetallic PdAu surface. The Pd enrichment increasing from Li^+ to Cs^+ was monitored by the decreasing concentration of CO adsorbed on Au than on Pd as well as the decreasing ratio between linear/bridged adsorbed CO and the increasing overall Pd/Au ratio derived from IR spectra. Table 1 compiles the surface concentrations [10^{-6} mol g^{-1}] and fractions [%] for CO adsorbed on PdAu/MOAc/SiO_2 calculated from absorption coefficients of CO on pure Au and Pd.[14]

The fractions of Au on PdAu, *i.e.*, "Au next to Pd" and "Au next to Au" decreased from 11% to 3% and from 33% to 8%, respectively, from the parent PdAu/SiO_2 to increasing main quantum number of the promoter. At the same time, the fraction of "Pd next to Pd" decreased from 45% to 30%, while that of "Pd next to Au" strongly increased from 11% to 59%. The significant increase of the band for CO on "Pd next to Au" is accompanied by a decrease of "Au next to Pd" from Li^+ to Cs^+. However, these bands are complementary and, thus, they should both either increase or decrease. The large shift in band position of "Pd next to Pd" and minor "Pd next to Au" to lower wavenumber (Fig. 2) and the behavior of "Pd next to Pd" (maximum fraction at Li^+) indicated that these Pd domains were in contact with MOAc. Due to these significant band shifts and broadenings, the bands assigned to "Pd next to Pd" and "Pd next to Au" are overlapping. As consequence (Table 1) the fraction of "Pd next to Pd" is underestimated and "Pd next to Au" is overestimated when going from Li^+ to Cs^+.

Therefore, the overall linear/bridged CO as well as the Pd/Au surface ratio was calculated using the absorption coefficients[14] of adsorbed CO on monometallic Au/SiO_2 and Pd/SiO_2. It decreased from 20.3 to 11.8, while the overall surface Pd/Au ratio increased from 3.1 to 8.5 when going from Li- to CsOAc. Acetates covalently bound to Li^+ show a lower strength of interaction with Pd in PdAu than acetates from CsOAc. The effect of acetate ions on PdAu and thus, the Pd surface enrichment increased towards CsOAc.

The effect of Pd surface enrichment upon promotion with MOAc depends on the overall as well as on the surface Pd/Au and the Pd/K^+ ratio. Previous studies[15] reveal the equilibrium between the Pd/MOAc layer and more or less soluble KPd-acetate species during vinyl acetate synthesis.[14] Independent from the synthesis procedure, PdAu particles undergo inter-diffusion already at room temperature[45] – during reaction, the thermodynamic stable Pd_1Au_1 phase is formed.

Having shown that MOAc induced PdAu particle reordering leads to an enrichment of Pd on the surface (increasing from Li to Cs acetate) under "non-reactive" heating, we investigate in the next step if the promoter has also an influence on the metal–metal distances.

3.2. Interaction of MOAc ($M^+ = Li^+$, Na^+, K^+, Cs^+) with Pd surface enriched PdAu

The influence of LiOAc on the structure of the bimetallic PdAu particles was further studied by EXAFS. Table 2 shows the metal–metal distances r and the coordination numbers N in PdAu/SiO_2 compared to PdAu/LiOAc/SiO_2 determined by multiple edge fitting with first shell analysis of Pd/Li^+ and Au/Li^+ contributions.

The addition of LiOAc to PdAu/SiO_2 enlarged the Pd–Pd distances compared to PdAu/SiO_2. The coordination numbers for Pd ($N_{PdM} = N_{PdPd} + N_{PdAu}$) and for Au ($N_{AuM} = N_{AuPd} + N_{AuAu}$) allow to distinguish a core–shell particle from one with a random alloy structure. In presence of a Pd enriched surface, N_{PdM} will be smaller than N_{AuM} because surface atoms have fewer neighbors than atoms in the core. On the other hand in a random alloy structure N_{PdM} is close to N_{AuM}.[33] The presence of Pd_1Au_1 phases can be deduced from a 2 : 1 ratio between N_{Pd-Pd} and N_{Pd-Au} (the same applies for the coordination numbers of Au).[16] For the samples studied, the total coordination numbers for Pd (~10) were lower than that of Au (~12), which indicates that Au occupied with preference sites in the core of the particles, while Pd atoms were located with preference on the surface. With the addition of LiOAc N_{PdPd} decreased from 7.9 to 7.1 indicating an enhanced surface segregation of Pd in presence of the promotor.

For $(PdAu)_{core}Pd_{shell}$ structures, the Pd atoms in the shell adopt the bond length of the Au atoms in the core up to a thickness of the shell approximating 1 nm.[33,46] On PdAu/LiOAc/SiO_2 the Pd–Pd distance was significantly longer by ~0.05 Å (2.75–2.80 Å) compared to the distances in PdAu/SiO_2, whereas mixed interatomic Pd–Au and Au–Pd distances increased only slightly from 2.77 to 2.78 Å. The Pd lattice expansion after LiOAc impregnation suggests the formation of a Pd/Li^+ mixed adlayer on the PdAu alloy particle.[16] First shell analysis of the EXAFS of the promoted sample indicates a Pd/Li^+ distance of 2.14 Å, which agrees well with the Pd and Li^+

Table 1 Surface concentrations [10^{-6} mol g^{-1}] and corresponding fractions [%] in brackets of CO adsorbed on PdAu/MOAc/SiO_2 after reaction (washed for 20 min)

PdAu/MOAc/SiO_2	Au next to Pd	Au next to Au	Pd next to Pd	Pd next to Au	Linear/bridged CO	Pd/Au
M^+ =	[10^{-6} mol g^{-1}] ([%])				[mol g^{-1}/mol g^{-1}]	
—	2.9(11)	8.7(33)	12(45)	3.0(11)	29.0	1.3
Li^+	3.0(6)	8.3(18)	25(54)	9.8(21)	20.3	3.1
Na^+	1.9(4)	5.9(14)	20(47)	15(35)	14.5	4.5
K^+	0.9(2)	4.9(12)	18(43)	18(44)	11.2	6.3
Cs^+	1.1(3)	3.2(8)	13(30)	24(59)	11.8	8.5

Table 2 Interatomic metal distances and coordination numbers in PdAu/SiO_2 and PdAu/LiOAc/SiO_2

	Au–Pd		Au–Au		Pd–Au		Pd–Pd		Pd–M^+	
Sample	*r*/Å	*N*	*r*/Å	*N*	*r*/Å	*N*	*r*/Å	*N*	*r*/Å	*N*
PdAu/SiO_2	2.77	4.5	2.80	7.3	2.77	2.2	2.75	7.9	—	—
PdAu/LiOAc/SiO_2	2.78	4.8	2.79	7.2	2.78	2.4	2.80	7.1	2.14	0.8

radii (r_{Pd} = 1.39 Å, r_{Li^+} = 0.75 Å). The small coordination number N_{Pd/Li^+} of 0.8, which averages over all Pd atoms present in the sample, additionally underlines that the Pd/Li^+ adlayer is formed as a thin shell on the alloy particle core.

The fit of the EXAFS oscillations improved significantly by including Pd/Li^+ contributions, while Au/Li^+ interactions were excluded as first shell analysis yielded nonrealistic parameters (*i.e.*, unacceptable distances and partly negative coordination numbers).

The changes in the interatomic Pd distances upon promoter impregnation and activation were first studied by XRD using the KOAc as model and then expanded to the other alkali acetates. The *in situ* XRD measured in N_2 flow in presence and absence of KOAc on mono- and on bimetallic catalysts is shown Fig. 3. The Pd(111) and Pd_xAu_y(111) diffraction peaks were observed between 36 and 42° 2θ for (a) PdAu/KOAc/SiO_2, (b) PdAu/SiO_2, (c) Au/KOAc/SiO_2 and (d) Pd/KOAc/SiO_2. On fresh PdAu/KOAc/SiO_2 catalysts, Au- and Pd-rich (Pd_0Au_{100}, $Pd_{89}Au_{11}$) as well as bimetallic particles composed of $Pd_{54}Au_{46}$ were observed (Fig. 3a).[14] While the Pd(111) reflex shifted from 40.0° to 39.3° 2θ after heating to 200 °C and further to 39.1° 2θ at 250 °C. The total shift of Pd(111) by $\Delta\theta$ = −0.9° to lower angles was irreversible upon cooling to room temperature. This KOAc induced shift in the Pd(111) reflex is attributed to the elongation of the Pd–Pd bond distance of ~0.055 Å, which is in good agreement with the increase in the Pd–Pd bond distance observed by EXAFS (~0.05 Å).

The temperature induced miscibility of bimetallic PdAu particles is independent of the presence of KOAc (Fig. 3b). The absence of a shift of the Au(111) peak in PdAu/KOAc/SiO_2 as well as in monometallic Au/KOAc (Fig. 3c) confirmed that the KOAc adsorption did not influence the Au–Au distance, while the Pd(111) diffraction peak shifted to lower angles by −1° after KOAc adsorption in monometallic Pd/KOAc/SiO_2 (Fig. 3d). The asymmetric shape of the Pd(111) reflection after cooling to 50 °C indicated the presence of two overlapping contributions at 39.26° and 40.05° 2θ (see Fig. 3e for the fit) corresponding to Pd–Pd distance enlargements of 0.055 Å and 0.002 Å. Consequently, *in situ* XRD results confirm the presence of a Pd/K^+ shell on Pd or PdAu implying that Pd migrates from the particle bulk to the alloy surface upon KOAc loading.

The next part addresses the question whether the Pd–Pd distance depends on the size of the promoter ions by comparing Li-, Na-, K- and Cs-acetate promoted PdAu/SiO_2 (Fig. S4, ESI§). In order to determine the starting temperature of the Pd–Pd bond expansion, the temperature was increased from 100 °C to 140 °C with steps of 10 °C allowing the system to equilibrate for 2 h at each temperature. The position of the Pd(111) peak was independent on the type of promoter. However, the temperature of the Pd–Pd bond expansion slightly decreased from 120 °C for PdAu/LiOAc/SiO_2 to 110 °C for Na-, K- and Cs-OAc impregnated PdAu/SiO_2. This indicates that the formation of the Pd/M^+ adlayer is accompanied by acetate decomposition to CO_x and H_2 catalyzed by Pd.[47] To test this hypothesis, the K^+ counter anion was varied from acetate to (non-decomposable) OH^-, CO_3^{2-}, $C_2O_4^{2-}$. The Pd–Pd bond enlargement increased in the order $OH^- < CO_3^{2-} < C_2O_4^{2-} < OAc^-$ (Fig. S5b, ESI§) underlining that Pd/M^+ formation is induced by counter ion transformation. As observed by *in situ* XRD (Fig. S5§), acetate as bidentate ligand favors the formation of the Pd/K^+–O layer of K^+ on the Pd surface

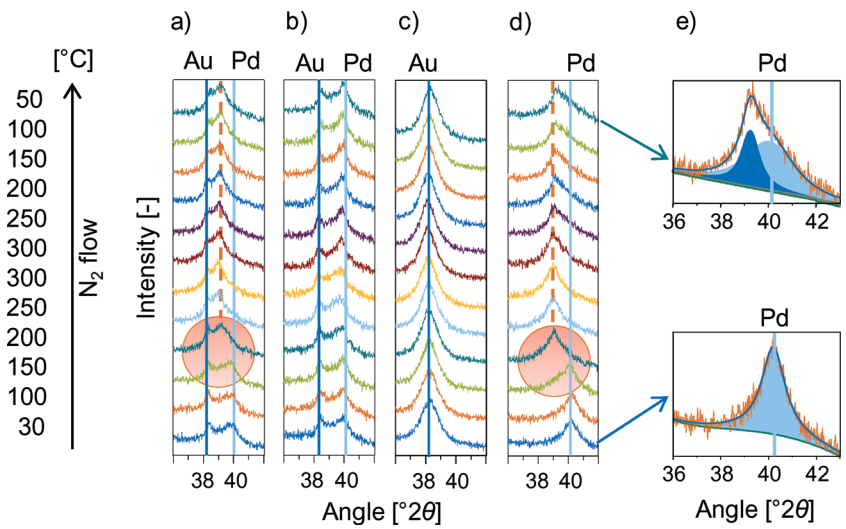

Fig. 3 *In situ* XRD profiles of Pd_xAu_y(111) for (a) PdAu/KOAc/SiO_2 (b) PdAu/SiO_2, (c) Au/KOAc/SiO_2, (d) Pd/KOAc/SiO_2 in flowing N_2 and (e) fits of Pd/KOAc/SiO_2 at 30 and 50 °C. The bimetallic phase is located between those of the pure metals: Au(111) (2θ = 38.3°, blue line) and Pd(111) (2θ = 40.1°, bright blue line).

layer of PdAu particles thereby favoring the dynamic reordering of PdAu by the formation of homogeneous $K_2Pd_2(OAc)_6$ species.[15]

Summarizing, IR, XAS and *in situ* XRD showed the temperature and counter ion dependent, but alkali cation radius independent formation of a Pd/M^+ adlayer on PdAu alloy particles. The formation of PdC_x, Pd hydride or Pd oxide species, which result in a similar Pd(111) peak shift,[48–51] was excluded by additional *in situ* XRD experiments in Fig. 4.

Adsorbed carbon from decomposed acetates[47,52] migrates to the Pd bulk to form PdC_x leading to a downshift of the Pd reflections corresponding to a Pd–Pd bond enlargement of 0.075 Å.[50,53] The presence of PdC_x instead of a Pd/K^+ mixed adlayer was not only excluded because of the difference in Pd bond enlargement (0.055 Å compared to 0.075 Å) but also by several independent experiments. $Pd(OAc)_2$ impregnated Pd/SiO_2 should show the Pd(111) shift in the absence of KOAc due to $Pd(OAc)_2$ decomposition that creates PdC_x. (Fig. 4a) Decomposition of thermally instable $Pd(OAc)_2$ above 140 °C led to the expected, however reversible in contrast to the irreversible Pd(111) shift for $PdAu/KOAc/SiO_2$. The absence of PdC_x from decomposed acetate was confirmed by applying NH_4OAc impregnated $PdAu/SiO_2$ (Fig. 4b). NH_4OAc decomposed, but generated tetragonal PdO at 34.0, 54.8 and 60.8° 2θ[54] and no shift of Pd(111) due to PdC_x. Additionally, possible PdC_x species in PdAu[51] can be removed by H_2 treatment at 180 °C.[55] Thus, $PdAu/KOAc/SiO_2$ was heated in N_2 to observe the downshift of Pd(111) and then in H_2 to remove possible PdC_x species (Fig. 4c). As expected, the Pd(111) peak shift occurred above 150 °C in N_2 but it was irreversible in H_2 strongly suggesting the absence of PdC_x.

Pd-hydride formation in H_2/N_2 as cause for the irreversible downshift of Pd(111) in $PdAu/KOAc/SiO_2$ is also excluded since hydrides decomposed above 150 °C leading to reversible Pd(111) shifts (Fig. 4d).

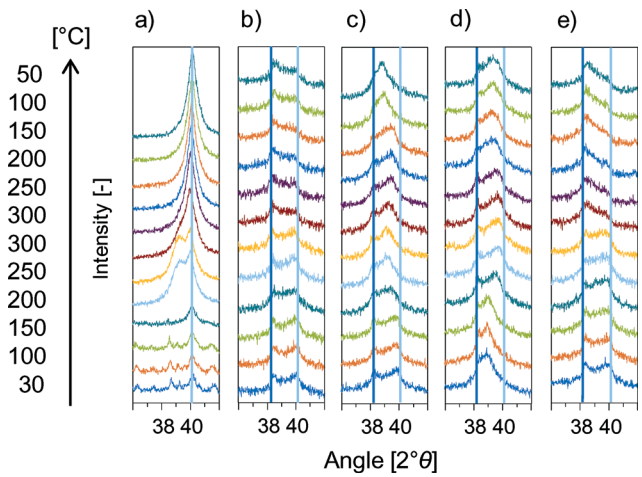

Fig. 4 Temperature dependent *in situ* XRD studies with (a) $Pd/Pd(OAc)_2$ in N_2, (b) $PdAu/NH_4OAc$ in N_2, (c) $PdAu/KOAc$ in N_2/H_2, (d) $PdAu/KOAc$ in H_2/N_2 and (e) $PdAu/KOAc$ in synthetic air. The bimetallic phase is located between those of the pure metals: Au(111) (2θ = 38.3°, blue line) and Pd(111) (2θ = 40.1°, bright blue line).

Formation of PdO on Pd(111)[56–59] was reported to form above 470 K and 2×10^{-2} Pa.[60] In order to check for PdO, *in situ* XRD was performed with $PdAu/KOAc/SiO_2$ in synthetic air (Fig. 4e). The Pd(111) reflex did not shift but became lower in intensity as soon as additional peaks for tetragonal PdO[54] formed. Consequently, the formation of bulk PdO can be excluded.

Summarily, our findings on the nature of interstitial PdC_x species, on Pd oxide and hydride species and the general finding that Au suppressed carbide formation in PdAu particles[61,62] led us to the conclusion that exclusively M^+ from MOAc (M^+ = Li^+, Na^+, K^+, Cs^+) induced the Pd–Pd bond enlargement. The fact that the Pd–Pd distance does not change as a function of the cation suggests that the cations form a surface layer on top of Pd inducing the elongation of the Pd–Pd distance in analogy to the widening of M–M distances increase upon hydrogen adsorption on metal nanoparticles.

3.3. Chemical composition and nature of the Pd/promoter$^+$ adlayer

Having shown that the migration of Pd to the PdAu particle surface and the formation of a mixed Pd/M^+ (M^+ = Li^+, Na^+, K^+, Cs^+) shell on the bimetallic PdAu core is induced by the presence of alkali acetates, we discuss the chemical nature of this adlayer.

Four locations of M^+ on $PdAu/MOAc/SiO_2$ can be considered, *i.e.*, (i) physisorbed MOAc species, (ii) interactions of M^+ with the silica support,[63] (iii) interaction of M^+ on the Pd/M^+ adlayer (Fig. 5) and (iv) binding of M^+ within the Pd/M^+ adlayer.

The samples were washed with water in order to differentiate the strength of interaction. It is expected that physisorbed MOAc species are easily removed by washing, while more strongly interacting M^+ ions on SiO_2 and on/in Pd/M^+ have higher stability. Thus, these components would be still detected after washing by chemical analysis of the washed $KOAc/SiO_2$ (concentration of K^+ in SiO_2) and $PdAu/KOAc/SiO_2$ samples (concentration of K^+ in SiO_2 plus Pd/M^+) (Table 3). All samples initially contained identical K^+ concentrations (~4.6 wt%); 0.208 wt% K^+ remained on washed $KOAc/SiO_2$ and a significant higher K^+ concentration (0.330 wt%) was found on washed $PdAu/KOAc/SiO_2$.

The difference in K^+ concentrations on both washed samples (0.122 wt%) allows to determine the K^+ concentration at or within the Pd/K^+ adlayer. With a dispersion of 24%

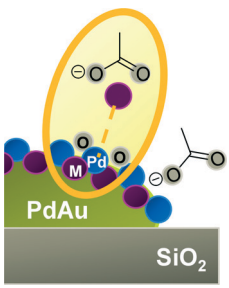

Fig. 5 Interaction of M^+ (violet) with the Pd/M^+ adlayer (blue/violet).

Table 3 Potassium concentrations on unwashed and washed $KOAc/SiO_2$ and $PdAu/KOAc/SiO_2$ after annealing to 300 °C

	Potassium concentration [wt%]	
Sample	Unwashed sample	Washed sample
$KOAc/SiO_2$	4.64	0.208
$PdAu/KOAc/SiO_2$	4.61	0.330

(average PdAu particle size of 3.6 nm), a Pd/Au molar surface ratio of 6.3 (from the IR spectrum of adsorbed CO[14]) and a total Pd loading of 1.4 wt%, about 2.7×10^{-5} mol Pd g^{-1} is located on the surface of the bimetallic particles. The agreement with the concentration of K^+ in Pd/K^+ (3.1×10^{-5} mol K^+ g^{-1}) indicates the formation of a Pd/K^+ monolayer with a ratio between K^+ and Pd surface atoms of ~1.

Having established the composition of Pd/K^+ as monolayer, its chemical nature was studied in more detail. To preserve the electroneutrality M^+ is expected to be in contact to oxygen species either in form of acetate or its oxidic decomposition products. In order to check for oxygen counter ions of K^+ in Pd/K^+, IR spectra of CO adsorbed on activated $PdAu/KOAc/SiO_2$ and $PdAu/KOH/SiO_2$ at 100 °C were compared (Fig. 6a and b). KOH, which partly forms K_2CO_3 in air, is stable in oxidic form on the catalyst surface during activation at 300 °C and, thus, the electronic influence of K^+ and O species on Pd can be observed by comparing the IR spectra of CO adsorbed on $PdAu/KOH/SiO_2$ and on $PdAu/KOAc/SiO_2$ at 100 °C. At this temperature, CO adsorbs only on Pd surface atoms in the bimetallic PdAu particles (Fig. S6, ESI§). Both spectra in Fig. 6 exhibited five CO bands between 2150 and 1600 cm^{-1} (Table 4). Linearly adsorbed CO on Pd sites has stretching frequencies of 2055 and ~2007 cm^{-1}. Bridged adsorbed CO on two neighboring Pd species appeared at 1937 cm^{-1} and the two CO bands at 1832 and 1780 cm^{-1} are attributed to threefold bridged adsorbed CO. Similar positions of the CO bands on both samples point to the formation of K^+-oxide species from KOAc during temperature treatment. The shift of the band for threefold bridged CO species to higher wavenumbers on $PdAu/KOH/SiO_2$ (1837 and 1788 cm^{-1}) compared to $PdAu/KOAc/SiO_2$ (1829 and 1773 cm^{-1}) can be attributed to local $CO–K^+$ interactions with KOH. This indicates that K^+ from KOH remains accessible for CO adsorption and is not "incorporated" into the Pd enriched PdAu surface. In contrast, K^+ from KOAc formed a mixed Pd/K^+ layer on PdAu. The lower ratio between linear and multifold adsorbed CO and the lower total Pd surface concentration (Table 4) on $PdAu/KOH/SiO_2$ compared with $PdAu/KOAc/SiO_2$ indicates that KOH covered and blocks the PdAu surface, whereas K^+ from KOAc was incorporated in the outer Pd layer of PdAu and generated the $Pd/K^+–O$ adlayer.

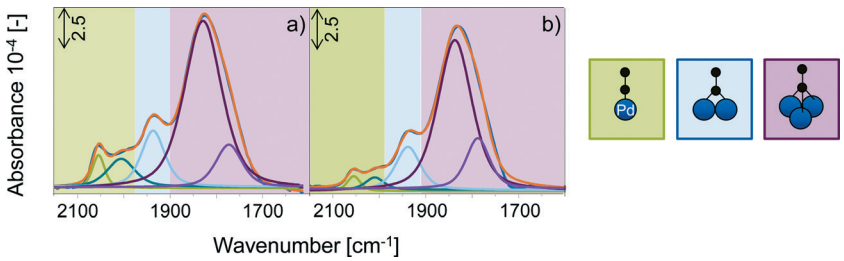

Fig. 6 IR spectra of 1.0 mbar CO adsorbed on (a) $PdAu/KOAc/SiO_2$ and on (b) $PdAu/KOH/SiO_2$ at 100 °C. Green bands are due to linearly adsorbed CO, the bright blue band is assigned to bridged adsorbed CO and violet bands to threefold hollow adsorbed CO.

Table 4 CO band positions, molar ratio of linear/bridged adsorbed CO ratio and total concentration of surface Pd sites on $PdAu/KOAc/SiO_2$ and $PdAu/KOH/SiO_2$ calculated from absorption coefficients of CO on Pd (ref. 14)

	Band positions [cm^{-1}]				
$PdAu/x/SiO_2$	Linear	Bridged	Threefold bridged	Linear/multifold	Concentration of Pd [10^{-5} mol g^{-1}]
KOAc	2055, 2006	1937	1829, 1773	3.5	2.3
KOH	2055, 2009	1938	1837, 1788	1.5	1.0

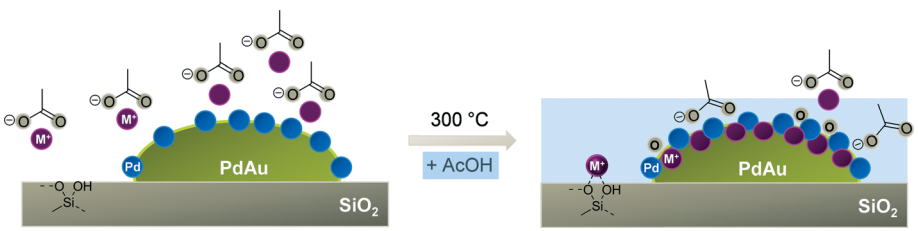

Fig. 7 Formation of the Pd/M^+-oxide adlayer on $PdAu/MOAc/SiO_2$ (M^+ = Li^+, Na^+, K^+, Cs^+) during activation and AcOH adsorption.

Fresh PdAu/MOAc/SiO_2 indicates partial oxidation of Pd either in form of Pd^+ or Pd^{2+} within the Pd/M^+–O adlayer which is supposed to be the precursor for homogeneous Pd^{2+}/M^+ acetate species in the reaction to vinyl acetate.

4. Conclusions

The promoters MOAc (M^+ = Li^+, Na^+, K^+, Cs^+) on PdAu/SiO_2 are located on the bimetallic particles as well as on the support (see Fig. 7). On SiO_2, MOAc forms M^+-silicates, while on the metal particles it induces the segregation of Pd to the surface of PdAu, generating a Pd/M^+-oxide adlayer during annealing. The formation of the Pd/K^+-oxide monolayer shell on PdAu particles exerts electronic and geometric changes in the catalysts accompanied by decomposition of acetates and leads to an increase in Pd–Pd bond length. These differences are characterized by two effects on Pd at the outermost layer. The Pd atoms, which are pulled out beyond the K^+ layer and form a "mixed" layer are located at irregular intervals (and do not contribute to the larger regular Pd–Pd distances). The Pd atoms enriched at the surface of the PdAu particle have an enhanced distance independent of the nature of the alkali cation, pointing to an unspecific interaction with the outer surface layer. Both Pd will contribute to catalysis, but with a rate significantly lower than the PdAu alloy. For VA synthesis, however, the Pd surface lattice mismatch modified by KOAc confines the reactants in small regions and limits in this manner side reactions. Additionally, the weakening of the interaction of the reactants with the metal sites enhances reaction selectivities and activities in the structure sensitive VA synthesis reaction.

Acknowledgements

Financial support by Wacker Chemie AG and fruitful discussions within the Wacker-Institut für Siliciumchemie is gratefully acknowledged. Xaver Hecht and Martin Neukamm are acknowledged for their experimental support.

References

1 M. Chen and D. W. Goodman, *Chin. J. Catal.*, 2008, **29**, 1178–1186.
2 M. S. Chen, K. Luo, T. Wei, Z. Yan, D. Kumar, C. W. Yi and D. W. Goodman, *Catal. Today*, 2006, **117**, 37–45.
3 A. E. Baber, H. L. Tierney and E. C. H. Sykes, *ACS Nano*, 2010, **4**, 1637–1645.
4 E. G. Allison and G. C. Bond, *Catal. Rev.*, 1972, **7**, 233–289.
5 H. P. Myers, L. Wallden and B. Karlsson, *Philos. Mag.*, 1968, **18**, 725–744.
6 D. Kumar, M. S. Chen and D. W. Goodman, *Catal. Today*, 2007, **123**, 77–85.
7 H. Okamoto and T. Massalski, *J. Phase Equilib.*, 1985, **6**, 229–235.
8 R. Elliott and F. Shunk, *J. Phase Equilib.*, 1982, **2**, 482–484.
9 A. Maeland and T. B. Flanagan, *Can. J. Phys.*, 1964, **42**, 2364–2366.
10 W. M. H. Sachtler and P. Van Der Plank, *Surf. Sci.*, 1969, **18**, 62–79.
11 L. Z. Mezey and J. Giber, *Jpn. J. Appl. Phys.*, 1982, **21**, 1569–1571.
12 R. Anton, H. Eggers and J. Veletas, *Thin Solid Films*, 1993, **226**, 39–47.
13 C. W. Yi, K. Luo, T. Wei and D. W. Goodman, *J. Phys. Chem. B*, 2005, **109**, 18535–18540.
14 E. K. Hanrieder, A. Jentys and J. A. Lercher, *ACS Catal.*, 2015, 5776–5786, DOI: 10.1021/acscatal.5b01140.
15 E. K. Hanrieder, A. Jentys and J. A. Lercher, *J. Catal.*, 2016, **333**, 71–77.
16 S. Simson, A. Jentys and J. A. Lercher, *J. Phys. Chem. C*, 2013, **117**, 8161–8169.
17 S. Simson, A. Jentys and J. A. Lercher, *J. Phys. Chem. C*, 2015, **119**, 2471–2482.
18 M. Chen, D. Kumar, C.-W. Yi and D. W. Goodman, *Science*, 2005, **310**, 291–293.
19 H.-J. Eberle, R. Heidenreich and J. Weis, *Ger. DE* 102006058800 A1, 2008.06.19, 2008.
20 L. Vegard, *Z. Phys.*, 1921, **5**, 17–26.
21 B. Ravel and M. Newville, *J. Synchrotron Radiat.*, 2005, **12**, 537–541.
22 W. K. Kuhn, J. Szanyi and D. W. Goodman, *Surf. Sci.*, 1992, **274**, L611–L618.
23 M. Mihaylov, K. Hadjiivanov and H. Knözinger, *Catal. Lett.*, 2001, **76**, 59–63.
24 T. Montanari, L. Castoldi, L. Lietti and G. Busca, *Appl. Catal., A*, 2011, **400**, 61–69.
25 T. Montanari, R. Matarrese, N. Artioli and G. Busca, *Appl. Catal., B*, 2011, **105**, 15–23.
26 T. P. Beebe, P. Gelin and J. T. Yates Jr, *Surf. Sci.*, 1984, **148**, 526–550.
27 M. Mihaylov, H. Knözinger, K. Hadjiivanov and B. C. Gates, *Chem. Ing. Tech.*, 2007, **79**, 795–806.
28 J. Shen, J. Hill, R. Watwe, S. G. Podkolzin and J. A. Dumesic, *Catal. Lett.*, 1999, **60**, 1–9.
29 E. L. Kugler and M. Boudart, *J. Catal.*, 1979, **59**, 201–210.
30 D. C. Meier and D. W. Goodman, *J. Am. Chem. Soc.*, 2004, **126**, 1892–1899.
31 E. Ozensoy and D. Wayne Goodman, *Phys. Chem. Chem. Phys.*, 2004, **6**, 3765–3778.
32 T. Wei, J. Wang and D. W. Goodman, *J. Phys. Chem. C*, 2007, **111**, 8781–8788.
33 F. Gao and D. W. Goodman, *Chem. Soc. Rev.*, 2012, **41**, 8009–8020.
34 D. Rainer, *J. Vac. Sci. Technol., A*, 1997, **15**, 1653–1662.
35 J. A. Rodriguez and D. W. Goodman, *Science*, 1992, **257**, 897–903.
36 Y.-S. Lee, Y. Jeon, Y.-M. Chung, K.-Y. Lim, C.-N. Whang and S.-J. Oh, *J. Korean Phys. Soc.*, 2000, **37**, 451–455.
37 C. T. Campbell and D. W. Goodman, *Surf. Sci.*, 1982, **123**, 413–426.
38 J. E. Crowell, E. L. Garfunkel and G. A. Somorjai, *Surf. Sci.*, 1982, **121**, 303–320.
39 J. E. Crowell and G. A. Somorjai, *Appl. Surf. Sci.*, 1984, **19**, 73–91.

40 E. L. Garfunkel, M. H. Farias and G. A. Somorjai, *J. Am. Chem. Soc.*, 1985, **107**, 349–353.
41 E. L. Garfunkel, J. E. Crowell and G. A. Somorjai, *J. Phys. Chem.*, 1982, **86**, 310–313.
42 E. L. Garfunkel and G. A. Somorjai, *Surf. Sci.*, 1982, **115**, 441–454.
43 A. F. Gusovius, T. C. Watling and R. Prins, *Appl. Catal., A*, 1999, **188**, 187–199.
44 F. Stoop, F. J. C. M. Toolenaar and V. Ponec, *J. Catal.*, 1982, **73**, 50–56.
45 A. Sellidj and B. E. Koel, *Phys. Rev. B: Condens. Matter Mater. Phys.*, 1994, **49**, 8367–8376.
46 A. Sárkány, O. Geszti and G. Sáfrán, *Appl. Catal., A*, 2008, **350**, 157–163.
47 M. Bowker, C. Morgan and V. P. Zhdanov, *Phys. Chem. Chem. Phys.*, 2007, **9**, 5700–5703.
48 S. Nakamura and T. Yasui, *J. Catal.*, 1970, **17**, 366–374.
49 S. A. H. Zaidi, *J. Catal.*, 1981, **68**, 255–263.
50 S. B. Ziemecki, G. A. Jones, D. G. Swartzfager, R. L. Harlow and J. Faber, *J. Am. Chem. Soc.*, 1985, **107**, 4547–4548.
51 M. Bonarowska, A. Malinowski, W. Juszczyk and Z. Karpiński, *Appl. Catal., B*, 2001, **30**, 187–193.
52 N. Aas and M. Bowker, *J. Chem. Soc., Faraday Trans.*, 1993, **89**, 1249–1255.
53 M. Bowker, C. Morgan and J. Couves, *Surf. Sci.*, 2004, **555**, 145–156.
54 J. Waser, H. A. Levy and S. W. Peterson, *Acta Crystallogr.*, 1953, **6**, 661–663.
55 M. Bonarowska, J. Pielaszek, V. A. Semikolenov and Z. Karpiński, *J. Catal.*, 2002, **209**, 528–538.
56 H. Conrad, G. Ertl, J. Küppers and E. E. Latta, *Surf. Sci.*, 1977, **65**, 245–260.
57 B. A. Banse and B. E. Koel, *Surf. Sci.*, 1990, **232**, 275–285.
58 S. Yang, A. Maroto-Valiente, M. Benito-Gonzalez, I. Rodriguez-Ramos and A. Guerrero-Ruiz, *Appl. Catal., B*, 2000, **28**, 223–233.
59 A. M. Venezia, L. F. Liotta, G. Pantaleo, V. La Parola, G. Deganello, A. Beck, Z. Koppány, K. Frey, D. Horváth and L. Guczi, *Appl. Catal., A*, 2003, **251**, 359–368.
60 E. H. Voogt, A. J. M. Mens, O. L. J. Gijzeman and J. W. Geus, *Surf. Sci.*, 1997, **373**, 210–220.
61 Y. F. Han, D. Kumar, C. Sivadinarayana, A. Clearfield and D. W. Goodman, *Catal. Lett.*, 2004, **94**, 131.
62 M. Bowker and C. Morgan, *Catal. Lett.*, 2004, **98**, 67.
63 M.-M. Pohl, J. Radnik, M. Schneider, U. Bentrup, D. Linke, A. Brückner and E. Ferguson, *J. Catal.*, 2009, **262**, 314–323.